RESEARCH MEMORANDUM

EFFECT OF CONVERGENT EJECTOR NOZZLES ON THE BOATTAIL DRAG OF A 16° CONICAL AFTERBODY AT MACH NUMBERS OF 0.6 TO 1.26

By James M. Cubbage, Jr.

Langley Aeronautical Laboratory
Langley Field, Va.

NATIONAL ADVISORY COMMITTEE
FOR AERONAUTICS

WASHINGTON

September 17, 1955
Declassified January 12, 1961

NATIONAL ADVISORY COMMITTEE FOR AERONAUTICS

RESEARCH MEMORANDUM

EFFECT OF CONVERGENT EJECTOR NOZZLES ON THE BOATTAIL DRAG OF A 16° CONICAL AFTERBODY AT MACH NUMBERS OF 0.6 TO 1.26*

By James M. Cubbage, Jr.

SUMMARY

An investigation has been conducted at Mach numbers of 0.6 to 1.26 to determine the effect of two convergent ejector-type nozzles with secondary weight flow ratios up to 0.36 on the drag of a 16° conical afterbody. The nozzles had ratios of secondary exit diameter to primary exit diameter of 1.1 and 1.375 and spacing ratios ranging from 0 to 1.6. Primary jet pressure ratios for these nozzles ranged from 2 to 8.

The results show that secondary flow rates greater than those usually required for cooling purposes did not have a large effect on the boattail drag coefficient; however, a trend to lower drag was noted as the amount of secondary flow increased. At primary jet pressure ratios corresponding to the design pressure ratio, the boattail drag coefficient increased with increasing spacing ratio up to a spacing ratio of about 0.8.

INTRODUCTION

The use of ejector-type exhaust nozzles on jet-propelled aircraft to provide cooling air for the tailpipe and nozzle in addition to some thrust augmentation has resulted in a number of investigations to determine the effect of various parameters on ejector performance. In considering the overall performance of this type of system, the effect of the jet from an ejector-type nozzle on afterbody drag must also be determined. Recent transonic investigations of jet effects on afterbody drag have, in general, been conducted with nonejector type of nozzles to simplify model construction and to expedite testing. Such investigations (for example, refs. 1 to 4 and others) have shown that the exhaust from a jet nozzle leads to large drag penalties under some conditions and that for other configurations large drag reductions were obtained. The

*Title, Unclassified.

addition of an ejector and its resulting secondary flow alters the flow configuration at the exit of the afterbody and thus possibly alters the effect of the jet flow on afterbody drag. References 3 to 6 contain experimental transonic data on afterbodies with ejector-type nozzles. These works include both isolated body and complete airplane configurations but the secondary flow rates investigated were generally restricted to the range required for adequate engine and tailpipe cooling. Ejector-type nozzles with secondary flow rates substantially greater than that required for cooling purposes have recently been considered for use as fixed geometry, variable-Mach number propulsive nozzles. In this application the secondary air flow is varied to control the expansion of the primary jet.

The present investigation was initiated to determine the drag characteristics of a boattailed afterbody with ejector-type nozzles operating at secondary weight flow rates as high as 36 percent of the primary flow and is part of an overall program in progress at the Langley Internal Aerodynamics Branch to study jet effects on afterbody drag at transonic speeds. The 16° conical afterbody model had a ratio of base diameter to maximum model diameter of 0.75 and the ratios of secondary to primary exit diameters of the two conical ejector nozzles used were 1.1 and 1.375. Data were recorded at spacing ratios of 0 to 1.6 at primary jet total pressure to free-stream static-pressure ratios up to 8. The nominal Mach numbers at which these data were recorded were 0.6, 0.9, 1.1, and 1.2, and the Reynolds number ranged from 3.4×10^6 per foot to 4.8×10^6 per foot.

SYMBOLS

$C_{D,\beta}$ boattail drag coefficient, $\frac{2}{r_m^2}\int_{r_b}^{r_m} -C_{p,\beta} r_x \, dr_x$

C_p pressure coefficient, $\frac{\frac{p}{p_\infty} - 1}{\frac{\gamma}{2} M_\infty^2}$

d diameter

p_t total pressure

$p_{t,j}/p_\infty$ primary jet total-pressure ratio

M Mach number

p static pressure

r radius

s distance between exit of primary nozzle and base of afterbody

T temperature, $^\circ R$

w weight flow

$\frac{w_s}{w_p}\sqrt{\frac{T_s}{T_p}}$ corrected weight flow ratio

x distance along center line of model from juncture of afterbody and model support tube

β boattail angle; angle between center line and a generatrix of model

γ ratio of specific heats

Subscripts:

b base

j jet

m maximum

s secondary

t total

p primary

∞ free stream

β boattail

APPARATUS AND TESTS

A sketch of the tunnel used in this investigation is presented as figure 1. This continuous-operation type of tunnel was used in previous investigations of jet effects and is described in detail in reference 7. The stream stagnation temperature at maximum Mach number was approximately 180° F.

The model support arrangement shown in figure 1 was described in reference 7. Air for both the primary and secondary flow was supplied from three 1,000-cubic-foot tanks which were pressurized to approximately 100 pounds per square inch. The temperature of the air supplied to the jet nozzle was approximately 70° F.

A simplified sketch of the ejector control mechanism and the secondary flow control valve is presented in figure 2. Photographs of the assembled control mechanism mounted in place are shown in figure 3. This mechanism provided remote adjustment of the spacing ratio and independent control of the secondary flow. Since no provisions were made in the secondary-flow control valve for an airtight seal when in the closed position, zero values of secondary to primary weight flow ratio were not obtained. In general, the minimum secondary-flow rate was on the order of 5 percent.

The model consisted of a 16° conical afterbody with a ratio of base diameter to maximum diameter of 0.75. The conically convergent ejector nozzle is shown in figure 4 with the two primary nozzles whose exit diameters were 1.0 inch and 1.25 inches. These diameters gave ratios of secondary exit diameter to primary exit diameter of 1.375 and 1.1, respectively. The design jet pressure ratios corresponding to these ratios of secondary to primary exit diameters were 3.05 and 5.24. Spacing ratios s/d_p of 0, 0.2, 0.4, 0.8, and 1.6 were used for each primary nozzle. The 16° afterbody was chosen as a compromise model that represented a structurally and mechanically desirable short afterbody with a reasonably good aerodynamic shape. Seven static pressure orifices 0.020-inch in diameter were located along a meridian of the boattail. The model was oriented in the tunnel so that these orifices were opposite the top slotted wall.

All pressures were measured by electrical pressure transducers, the outputs of which were transferred to line traces on paper film by a recording oscillograph. Several of these pressures were recorded visually from manometer tubes at each test point. The secondary weight flow was determined from the pressure drop in a 2-foot section of the annular secondary air passage which was independently calibrated against a venturi meter prior to the start of the tests; for this calibration the primary jet was plugged. A flow coefficient of 0.96 obtained from

total-pressure surveys of the primary nozzle was applied to the computed primary weight flow. Since the primary and secondary air came from a common source, the temperature correction factor $\sqrt{\frac{T_s}{T_p}}$ equaled 1.0.

Inasmuch as the test setup was the same as that reported in references 2 and 7, the boundary-layer thickness on the model and support pipe was assumed to be the same. Results presented in reference 7 showed the boundary-layer thickness $5\frac{1}{2}$-inches upstream of the model base to be approximately 0.4-inch or 20 percent of the maximum model diameter; the corresponding displacement thickness was 0.05-inch.

RESULTS AND DISCUSSION

Boattail Pressure Distributions

Static-pressure-coefficient distributions along the boattail for several values of primary jet pressure ratio, corrected weight flow ratio, spacing ratio, and Mach number are presented as figure 5. These distributions are typical of those measured for other test conditions. The two values of $\frac{w_s}{w_p}\sqrt{\frac{T_s}{T_p}}$ shown for each value of primary jet pressure ratio are the minimum and maximum for these test conditions. Distributions obtained on a similar afterbody with a simple nozzle (ref. 2) are also shown in the figure at $s/d_p = 0$.

The distributions for $M_\infty = 0.9$ in figure 5(a) are typical of unseparated flow over a body of this type; that is, the external flow accelerates rapidly in negotiating the cone-cylinder juncture and then compresses rapidly at first and more slowly as it progresses along the boattail. In figure 5(b) the distributions for certain test conditions, $M_\infty = 1.26$, $s/d_p = 1.6$, and $p_{t,j}/p_\infty = 4$ and 6, for example, show a rapid increase in pressure coefficient $\left(C_{p,\beta}\right.$ becomes less negative$\left.\right)$ occurring at various distances along the afterbody. At other test conditions the increase in pressure coefficient along the boattail is more gradual. The abrupt increase in $C_{p,\beta}$ indicates separation of the flow from the boattail at these points whereas the more gradual increase in pressure coefficient over the boattail indicates that the flow remained attached.

The effect of increasing $\frac{w_s}{w_p}\sqrt{\frac{T_s}{T_p}}$ on the distributions of figure 5 is seen to be a general increase in pressure over the entire boattail at $M_\infty = 0.9$ but it is restricted to the rearward part of the boattail at $M_\infty = 1.26$. It will also be noted in this figure that except near the cone-cylinder juncture the pressure coefficients are generally greater than those of reference 2. The consistent difference between the distributions for maximum and minimum secondary flow at $M_\infty = 0.9$ is not completely understood. Any effect of the larger amount of secondary flow would be expected to be greatest near the base (as in the case at supersonic speeds) and progressively less farther up on the boattail. The data indicate, however, that the increase in pressure at the base due to the larger corrected weight flow is felt along the entire length of the afterbody. It should be pointed out that the maximum variation in $p_{t,j}/p_\infty$ between the two values of $\frac{w_s}{w_p}\sqrt{\frac{T_s}{T_p}}$ for a given spacing ratio is 0.10, the average difference being 0.03. Similarly, the maximum difference in Mach number is 0.007 with an average difference of about 0.004.

Boattail Drag Coefficient

The pressure drag of a boattailed afterbody consists of the pressure drag of the boattail and the pressure drag of the base of the afterbody. Previous investigations of afterbody drag (ref. 2, for example) have shown that, depending upon the afterbody geometry, the base drag can represent a substantial percentage of the total afterbody pressure drag in one case and in another case the base pressure can be above ambient and thereby produce a thrust. The data of reference 2 showed that for a 16° afterbody similar to the model of the present investigation the base drag was about 10 percent of the afterbody drag at supersonic speeds and at subsonic speeds the base pressure was close to or above ambient. On the basis of these conditions and the small base area of the model, it was decided to neglect the base drag for this investigation and to measure pressures on the boattail only. The thrust component represented by above-ambient pressures in the secondary exit are considered to be part of the ejector thrust and hence do not appear in these data.

Effect of secondary corrected weight flow ratio.- The basic results of this investigation are presented in figure 6 and 7 in the form of boattail drag coefficient $C_{D,\beta}$ as a function of $\frac{w_s}{w_p}\sqrt{\frac{T_s}{T_p}}$ at constant

values of primary jet pressure ratio and Mach number. Curves for the ejector nozzle with a diameter ratio $\frac{d_s}{d_p}$ of 1.375 are presented in figure 6 and for the nozzle with a diameter ratio of 1.10 in figure 7. Sketches of the nozzle configuration are shown for each spacing ratio to facilitate visualization of the geometry. The range of corrected weight flow ratio in these figures varies with primary jet pressure since a common source was used for both primary and secondary flows; the smaller range of secondary flow shown in figure 7 $\left(\frac{d_s}{d_p} = 1.10\right)$ results from the much smaller secondary exit area.

The effect of secondary flow on the boattail drag coefficient was small with a general trend to lower drag noted for both models as $\frac{w_s}{w_p}\sqrt{\frac{T_s}{T_p}}$ increased. In a few cases (fig. 6(d) at a spacing ratio of 0.2, for example) the effect of secondary corrected weight flow ratio on $C_{D,\beta}$ is reversed or nonexistent. Although the change in boattail drag is shown to be generally small coefficientwise in figures 6 and 7, in terms of percent of engine thrust for a set of assumed conditions it represents a significant figure. For example, on a 6-foot-diameter body flying at $M_\infty = 0.9$ at sea level, 0.01 change in boattail drag coefficient equals about 100 pounds or 1 percent of a 10,000-pound-thrust engine. For the 1.375 ejector nozzle (fig. 6) the decrease in boattail drag coefficient with increasing corrected weight flow ratio is generally greater at low values of spacing ratio. This is not apparent for the 1.10 nozzle of figure 7 where the effects of secondary flow were very small.

The effect of a jet on flow over the afterbody from which it issues has been shown in previous investigations to depend upon (1) its tendency to reduce pressures in the dead-air region of the base through mixing along the jet boundary and (2) upon the extent to which the external stream is compressed as it is deflected away from the body axis by the presence of the jet. The presence of a low-velocity secondary stream surrounding the high-velocity jet core reduces the pumping effectiveness of the latter and increases the external interference between the jet flow and external flow. Since both effects should be favorable, it is not surprising that the afterbody drag generally decreases with increasing secondary flow. The magnitude of the effect, however, is smaller than might have been anticipated and the absence of a favorable secondary flow effect in several tests suggests that other, as yet undetermined, factors are influencing the flow.

Effect of ejector spacing ratio.- In figures 8 and 9 the variation of boattail drag coefficient with spacing ratio is shown for selected values of secondary corrected weight flow ratio. These curves are cross plots of the basic data presented in figures 6 and 7. The symbols on these figures are used only to identify the curves and do not necessarily represent actual test points.

At both subsonic and supersonic speeds (figs. 8 and 9), the effect of spacing ratio on boattail drag was generally small at the lower jet pressure ratios. Above a Mach number of 0.6 the boattail drag coefficient for the smaller primary nozzle (fig. 8) increased with increasing spacing ratio at $p_{t,j}/p_\infty = 4$ and above with the maximum drag occurring at $s/d_p \approx 0.8$. At a jet pressure ratio of 8, for example, the boattail drag coefficient increased as much as 0.07 as s/d_p increased from 0 to 0.8. At lower jet pressures the boattail drag coefficient remained about constant above $s/d_p = 0.8$ whereas at the higher jet pressure $C_{D,\beta}$ generally decreased a small amount above $s/d_p = 0.8$. It is of interest to note here that investigations of ejector nozzle performance have shown that maximum gross thrust of this type nozzle occurs over a range of spacing ratios from 0.8 to 1.2.

These same general effects of spacing ratio are noted for the larger diameter primary nozzle of figure 9 although they are reduced in magnitude. It will also be noted in figures 8 and 9 that the level of the boattail drag coefficient was reduced by increasing the primary nozzle diameter. This result is in agreement with results from other investigations such as references 2 and 7.

The variation of boattail drag coefficient with spacing shown in figure 8 would be expected if the predominant factor controlling the effect of the jet on afterbody drag is the amount of interference between the jet flow and the external flow. That is, at $s/d_p = 0$ the bulb created by the expanding jet, at a pressure ratio of 6, for instance, would cause a greater amount of interference (because of the turning of the external flow through a greater angle) than would occur for a spacing ratio greater than zero. Upon reaching a spacing ratio of 0.8 or greater, the jet boundary near the base must be nearly parallel to the axis of the model and thus any interference between the two flows is reduced to a minimum. At jet pressure ratios above the design pressure ratio, the jet would continue to expand upon reaching the base of the model. The amount of this expansion at the base would depend on the jet pressure and the amount of secondary flow, but in any case the resulting interference between the jet and external flows would probably be less than that for the same conditions at $s/d_p = 0$. The smaller effect of spacing ratio on the boattail drag of the model with the 1.10 nozzle (fig. 9) is judged to result from the interference effect between the two flows

having reached a maximum with the increase in primary nozzle diameter. Consequently, any variations in the angle between the jet boundary and the axis of the model would have relatively little effect on the amount of interference between the jet flow and external flow.

Effect of primary jet pressure ratio.- The variation of boattail drag coefficient with primary jet total-pressure ratio is shown in figure 10 for the $\frac{d_s}{d_p} = 1.375$ nozzle. Again the symbols are used to identify the curves and do not necessarily represent actual test points. The boattail drag coefficient, at spacing ratios less than 0.8, decreased with increasing primary pressure ratio. At $s/d_p \leq 0.8$, the change in drag with increasing $p_{t,j}/p_\infty$ was small and at $M_\infty = 0.6$ and 0.9, the data for most secondary flow rates show an increasing boattail drag above a pressure ratio of 4. At supersonic speeds (figs. 10(c) and 10(d)) the boattail drag coefficient generally decreases at a greater rate with increasing jet pressure ratio. It will be noted in figures 10(c) and (d) that, above $s/d_p = 0.4$, the beneficial interference effect of the jet is delayed until pressure ratios on the order of 8 are reached. At these pressure ratios the ejector nozzle was underexpanded and the jet underwent a second expansion upon reaching the exit of the model. As mentioned in previous sections, this second expansion causes a decrease in drag in the same manner as observed at zero or small spacing ratios. As the secondary flow is increased, the initial expansion of the primary jet is restricted somewhat and a greater expansion at the exit of the model results.

The curves of figure 10 are very similar to those obtained in previous work with a simple convergent nozzle. This is shown in figure 11 where interpolated data from reference 2 has been plotted with $s/d_p = 0$ data from this investigation. The data from reference 2 are presented as the zero secondary-flow case; thus, the effect of secondary-flow rate on $C_{D,\beta}$ is shown over a range from 0 to 20 percent. From the drag standpoint alone, the zero-length ejector shows a clear superiority over other configurations. For this configuration the afterbody drag coefficient at the higher jet pressure ratios was reduced 0.05 by introduction of secondary flow equal to 20 percent of the primary flow.

SUMMARY OF RESULTS

An investigation of the effect of an ejector-type nozzle on the boattail drag coefficient of a 16° conical afterbody at Mach numbers of 0.6 to 1.26 yielded the following results:

1. For the model of this investigation secondary-flow rates greater than those usually required for nozzle cooling purposes (approximately 3 percent) did not have a large effect on the boattail drag coefficient. A trend toward lower drag was noted with increasing amounts of secondary flow up to 36 percent of the primary flow.

2. For primary jet pressure ratios corresponding to the design pressure ratio of the nozzle, the boattail drag increased with increasing spacing ratio up to a spacing ratio of 0.8. Depending upon the test conditions and the diameter of the primary nozzle, this increase in boattail drag coefficient ranged from 13 to about 50 percent.

Langley Aeronautical Laboratory,
National Advisory Committee for Aeronautics,
Langley Field, Va., July 11, 1958.

REFERENCES

1. Henry, Beverly Z., Jr., and Cahn, Maurice S.: Preliminary Results of an Investigation at Transonic Speeds To Determine the Effects of a Heated Propulsive Jet on the Drag Characteristics of a Related Series of Afterbodies. NACA RM L55A24a, 1955.

2. Cubbage, James M., Jr.: Jet Effects on the Drag of Conical Afterbodies for Mach Numbers of 0.6 to 1.28. NACA RM L57B21, 1957.

3. Pel, C., and Rustemeyer, A.: Investigation of Turbojet Exhaust-Interference Drag. Report R-0801-12, United Aircraft Corp. Res. Dept., Nov. 1955.

4. Salmi, Reino J.: Experimental Investigation of Drag of Afterbodies With Exiting Jet at High Subsonic Mach Numbers. NACA RM E54I13, 1954.

5. Norton, Harry T., Jr., and Swihart, John M.: Effect of a Hot-Jet Exhaust on Pressure Distributions and External Drag of Several Afterbodies on a Single-Engine Airplane Model at Transonic Speeds. NACA RM L57J04, 1958.

6. Gorton, Gerald C.: Pumping and Drag Characteristics of an Aircraft Ejector at Subsonic and Supersonic Speeds. NACA RM E54D06, 1954.

7. Cubbage, James M., Jr.: Jet Effects on Base and Afterbody Pressures of a Cylindrical Afterbody at Transonic Speeds. NACA RM L56C21, 1956.

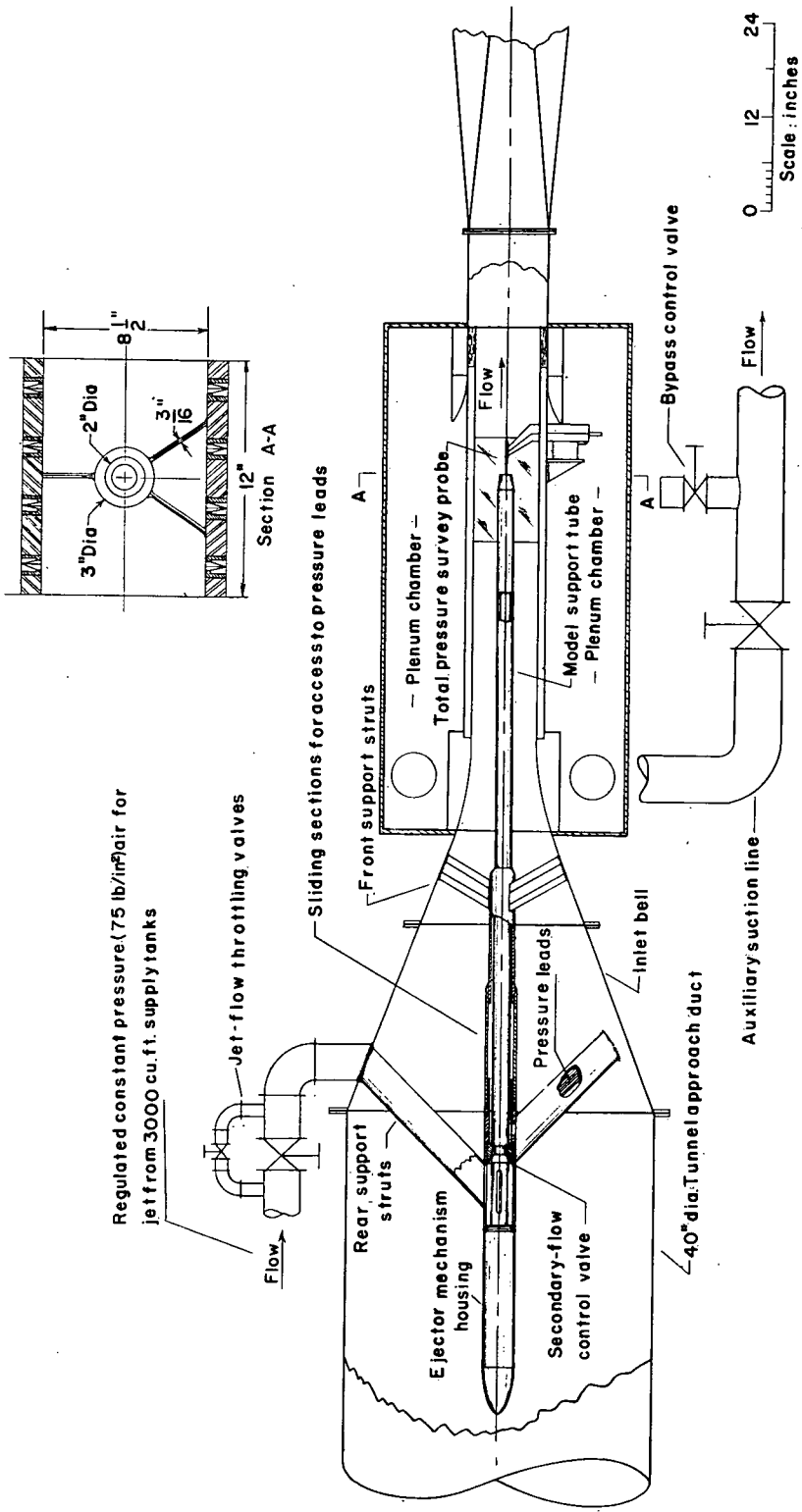

Figure 1.- Drawing of tunnel and model support arrangement.

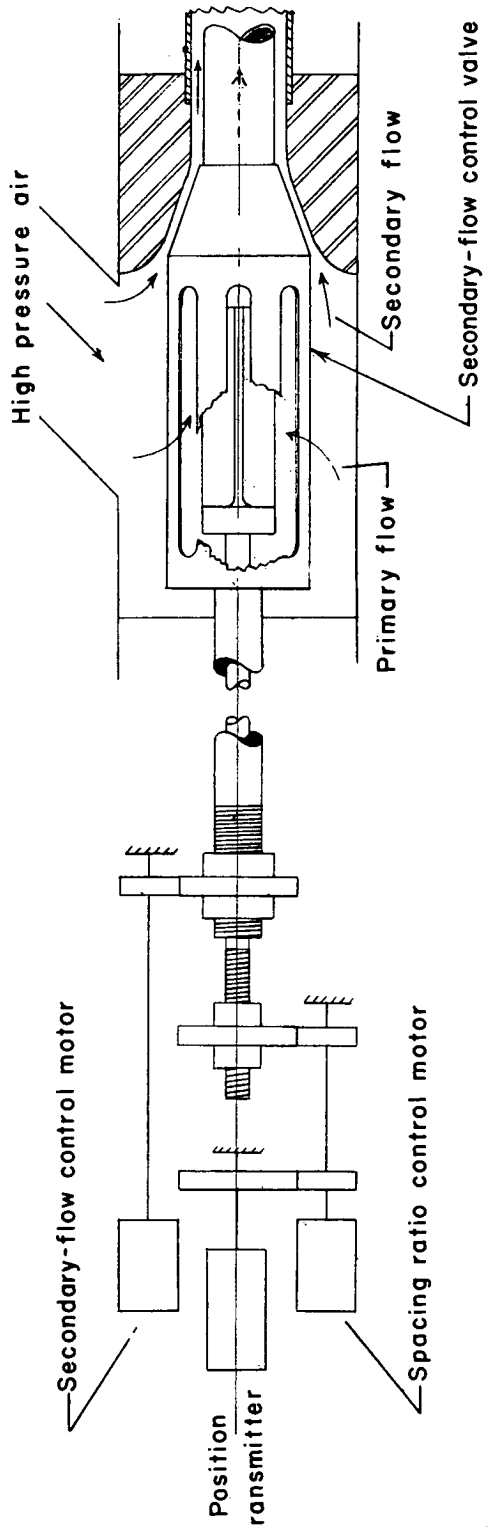

Figure 2.- Drawing of ejector control mechanism and model support tube.

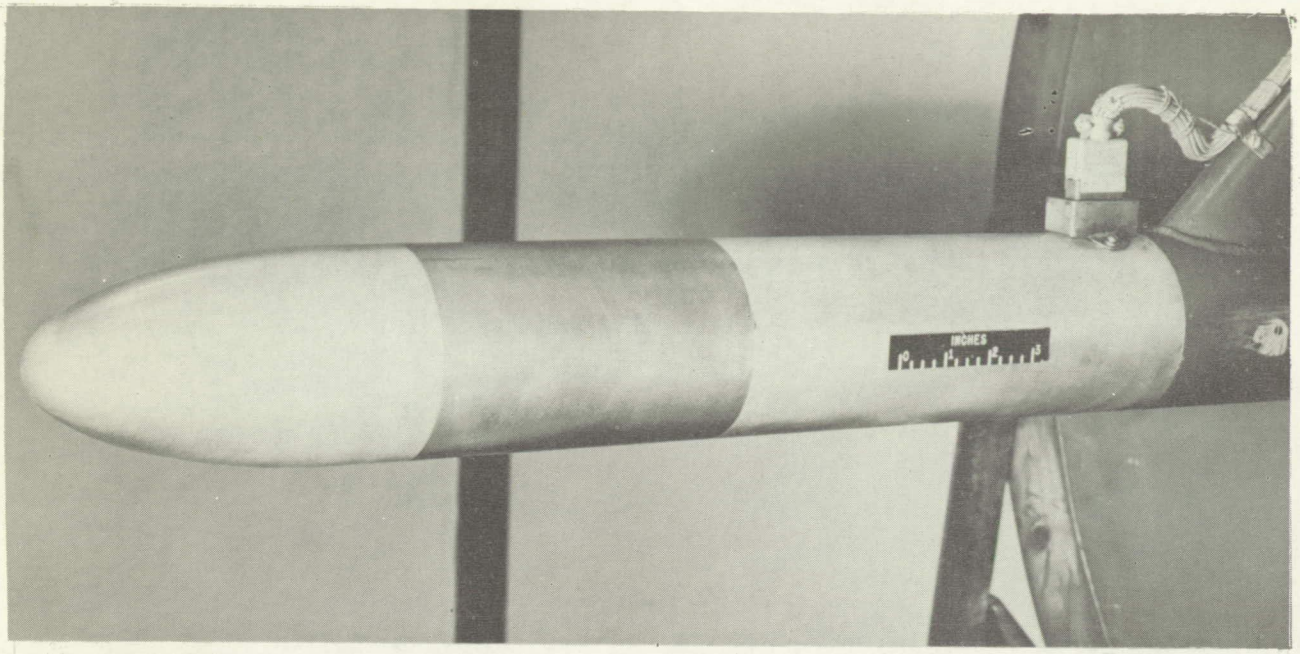

L-57-2870

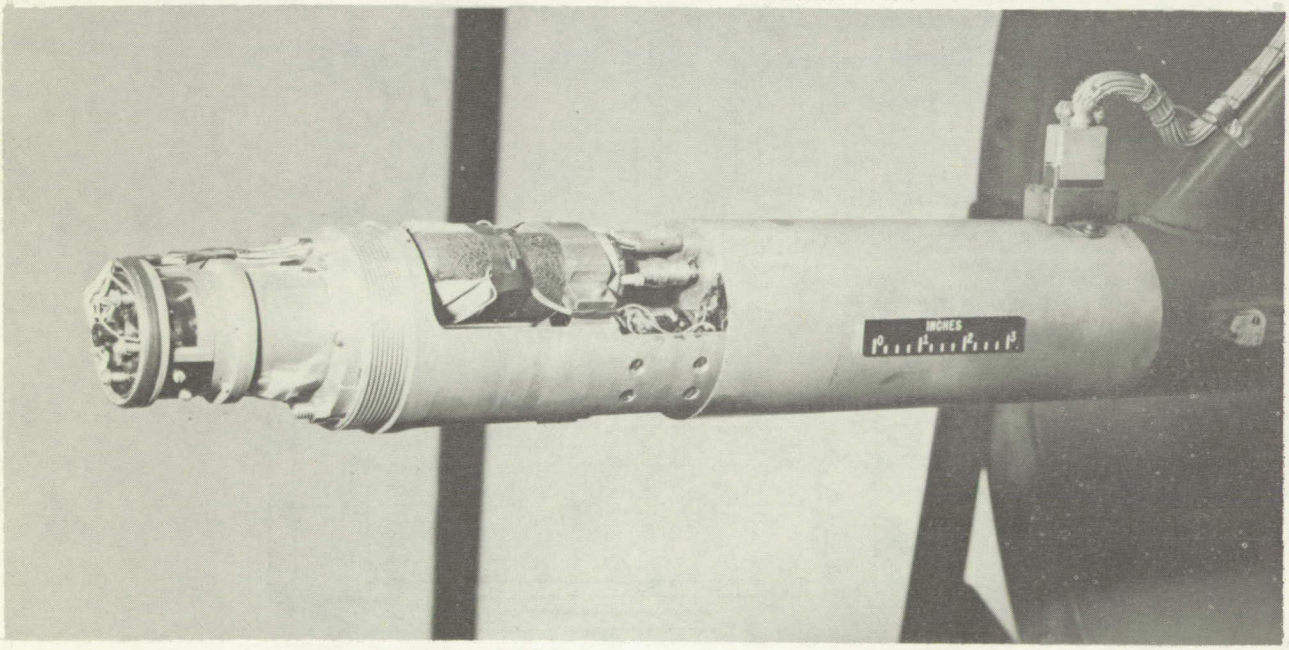

L-57-2871

Figure 3.- Photographs of ejector control mechanism mounted in place.

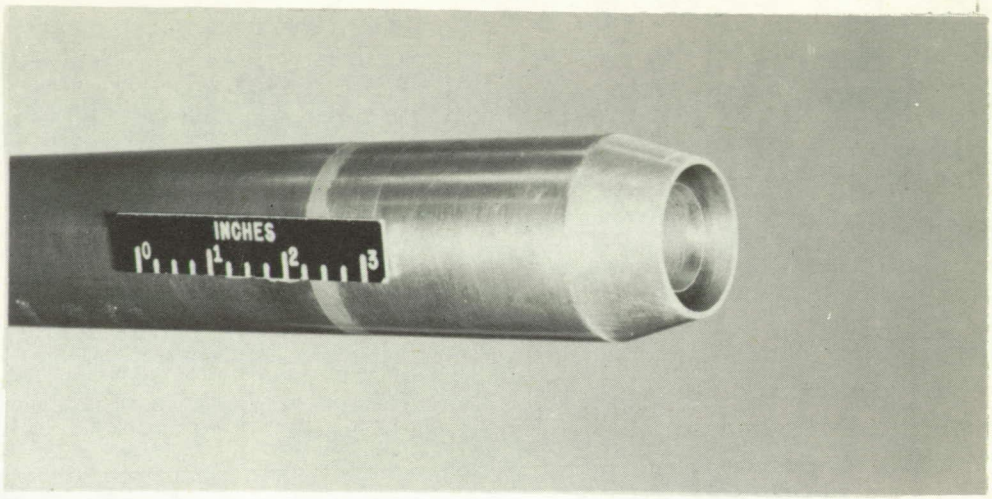

L-57-2869

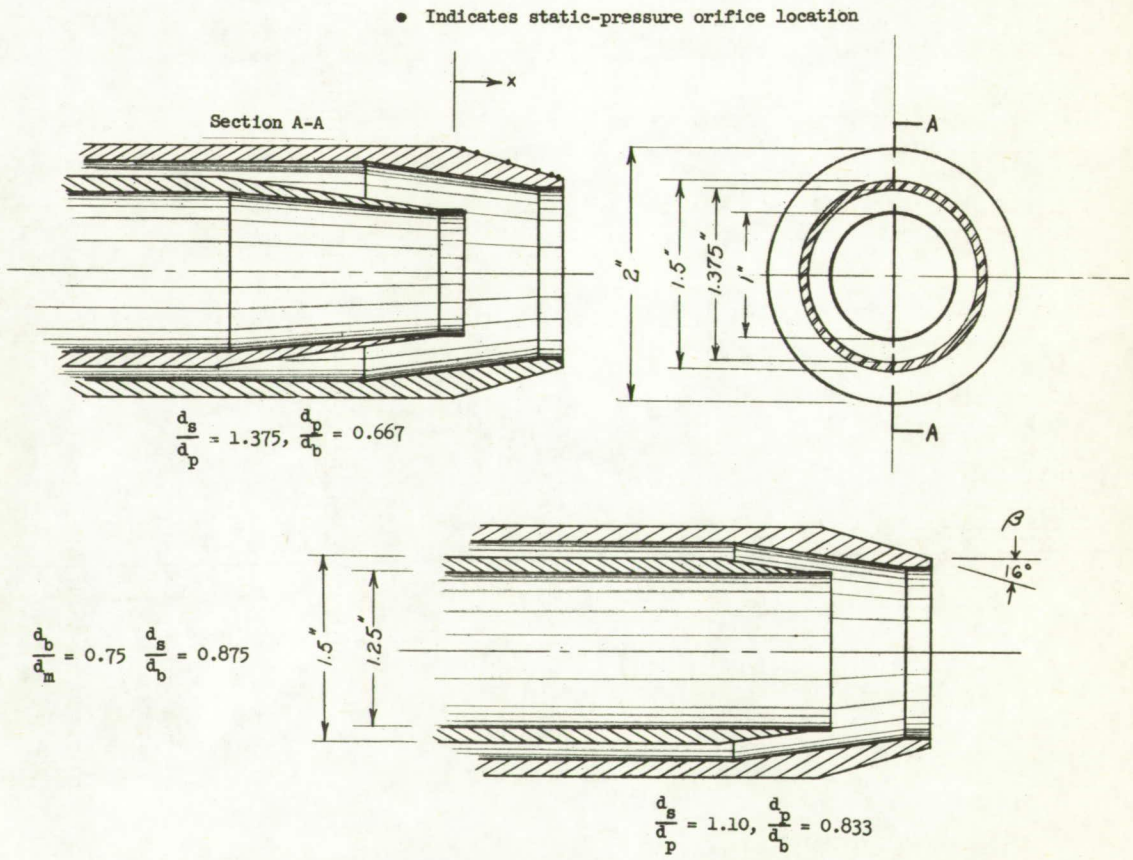

Figure 4.- Photograph and drawing of afterbody and ejector nozzles.

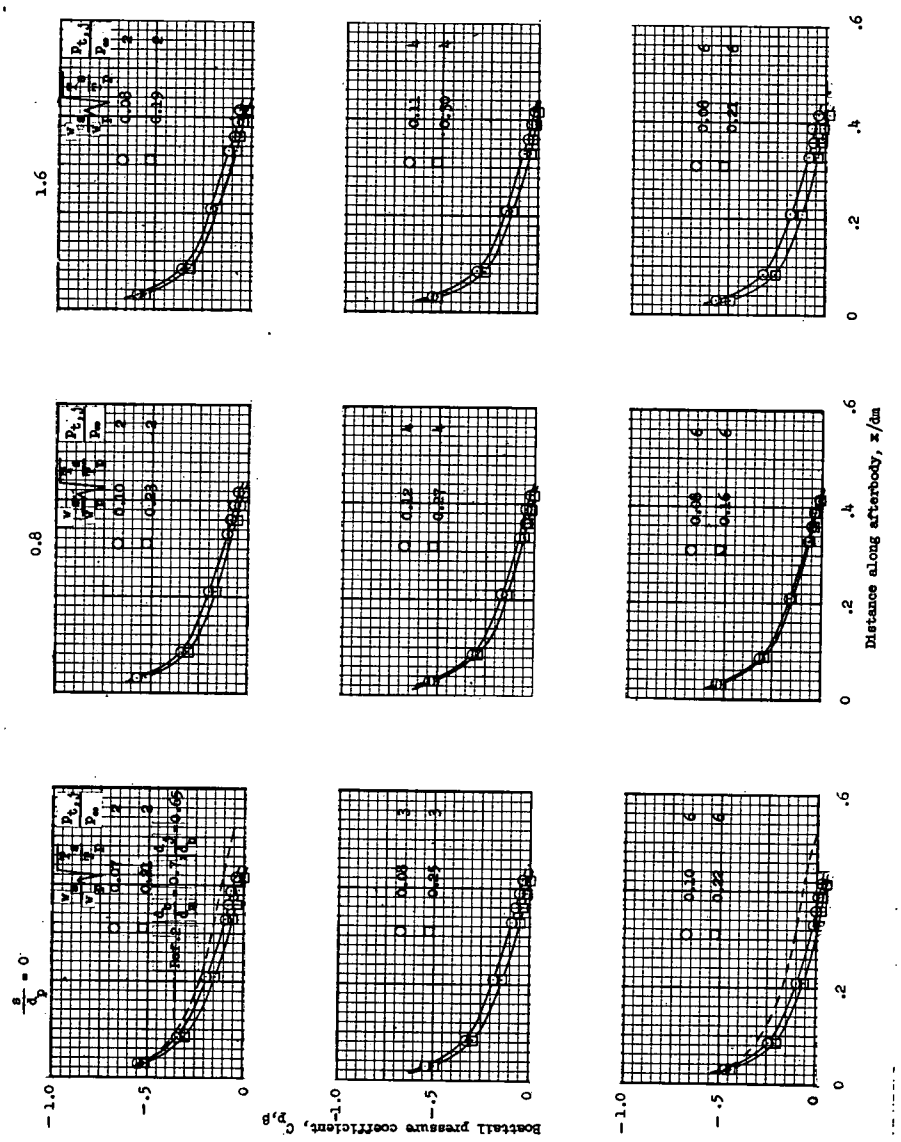

(a) $M_\infty = 0.9$.

Figure 5.- Typical boattail pressure-coefficient distributions. $\frac{d_s}{d_p} = 1.375$; $\beta = 16^\circ$.

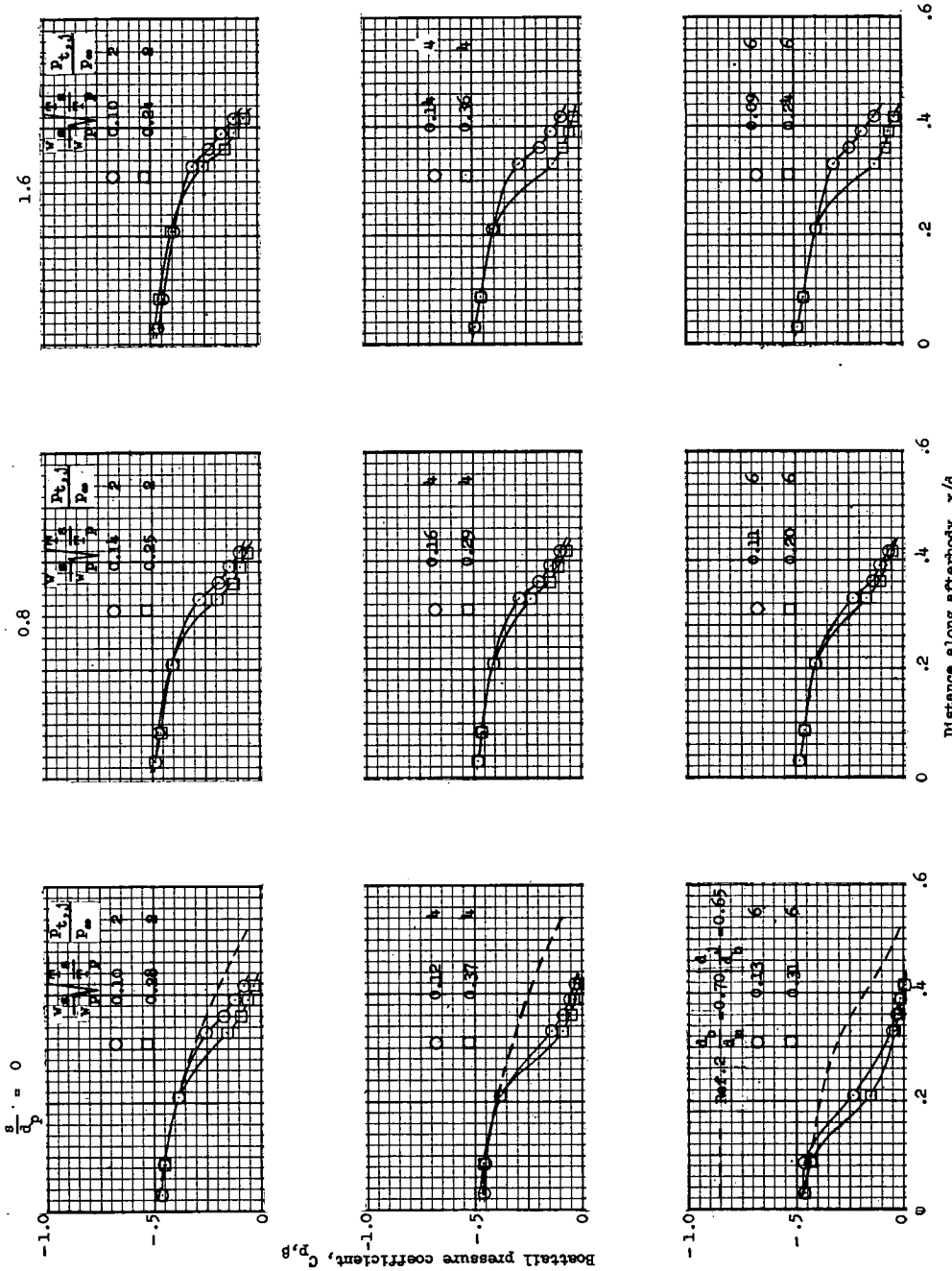

(b) $M_\infty = 1.26$.

Figure 5.- Concluded.

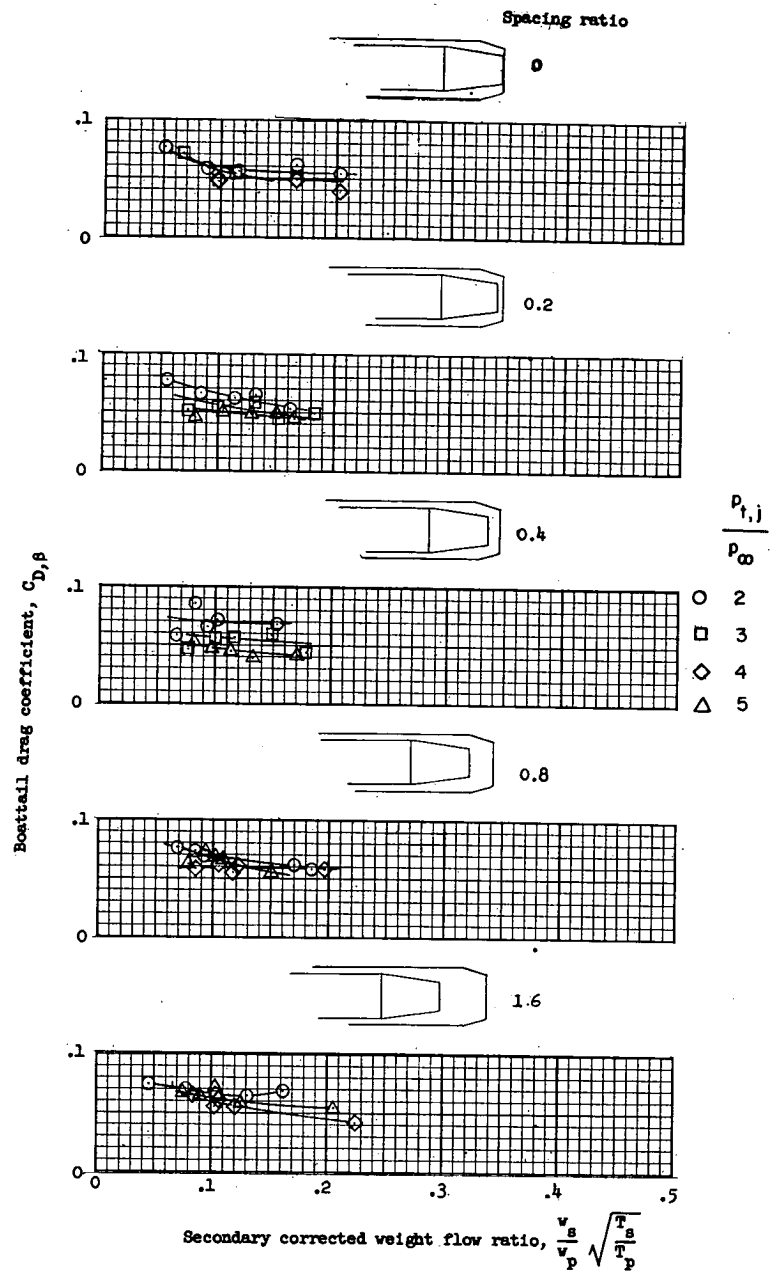

(a) $M_\infty = 0.6$.

Figure 6.- Variation of boattail drag coefficient with corrected weight flow ratio at constant values of primary jet total-pressure ratio and spacing ratio. $\frac{d_s}{d_p} = 1.375$.

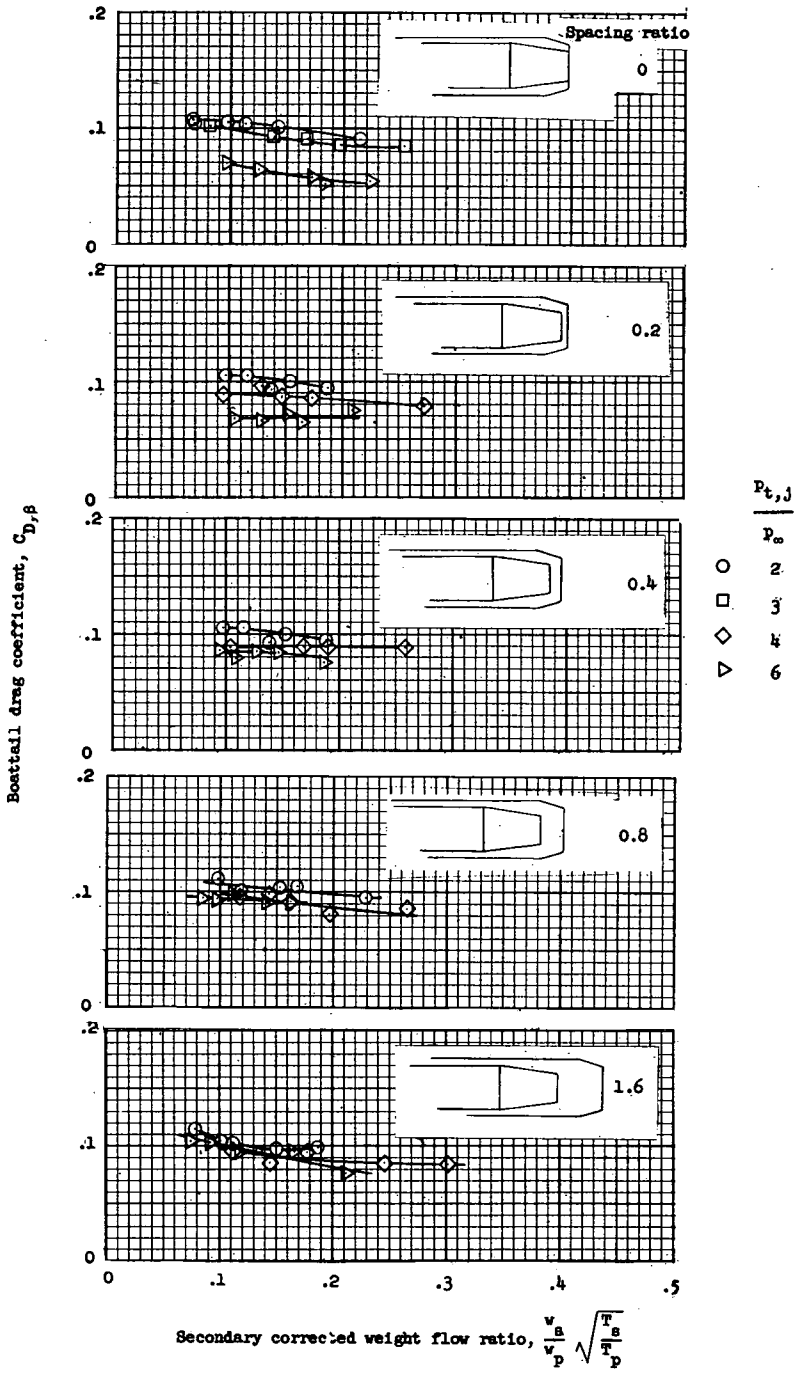

(b) $M_\infty = 0.9$.

Figure 6.- Continued.

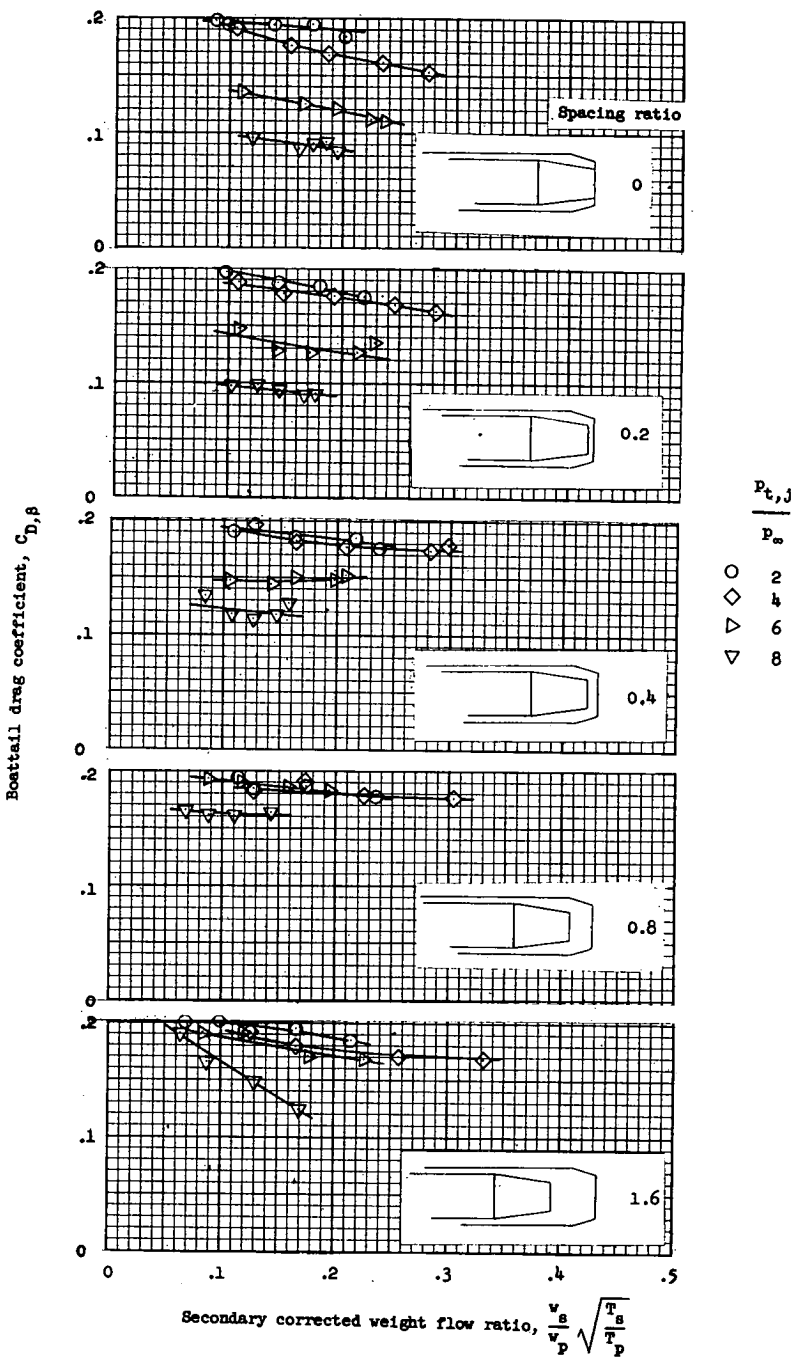

(c) $M_\infty = 1.10$.

Figure 6.- Continued.

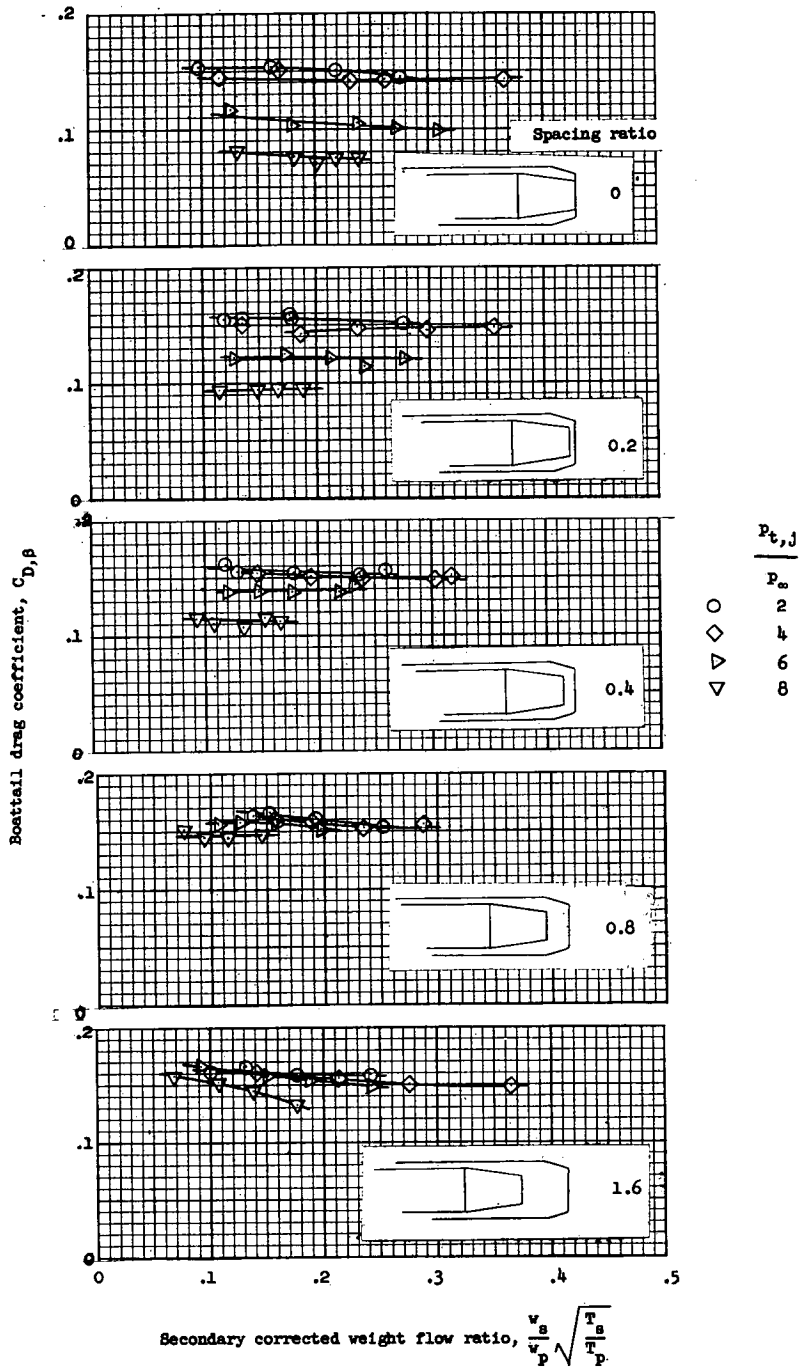

(d) $M_\infty = 1.26$.

Figure 6.- Concluded.

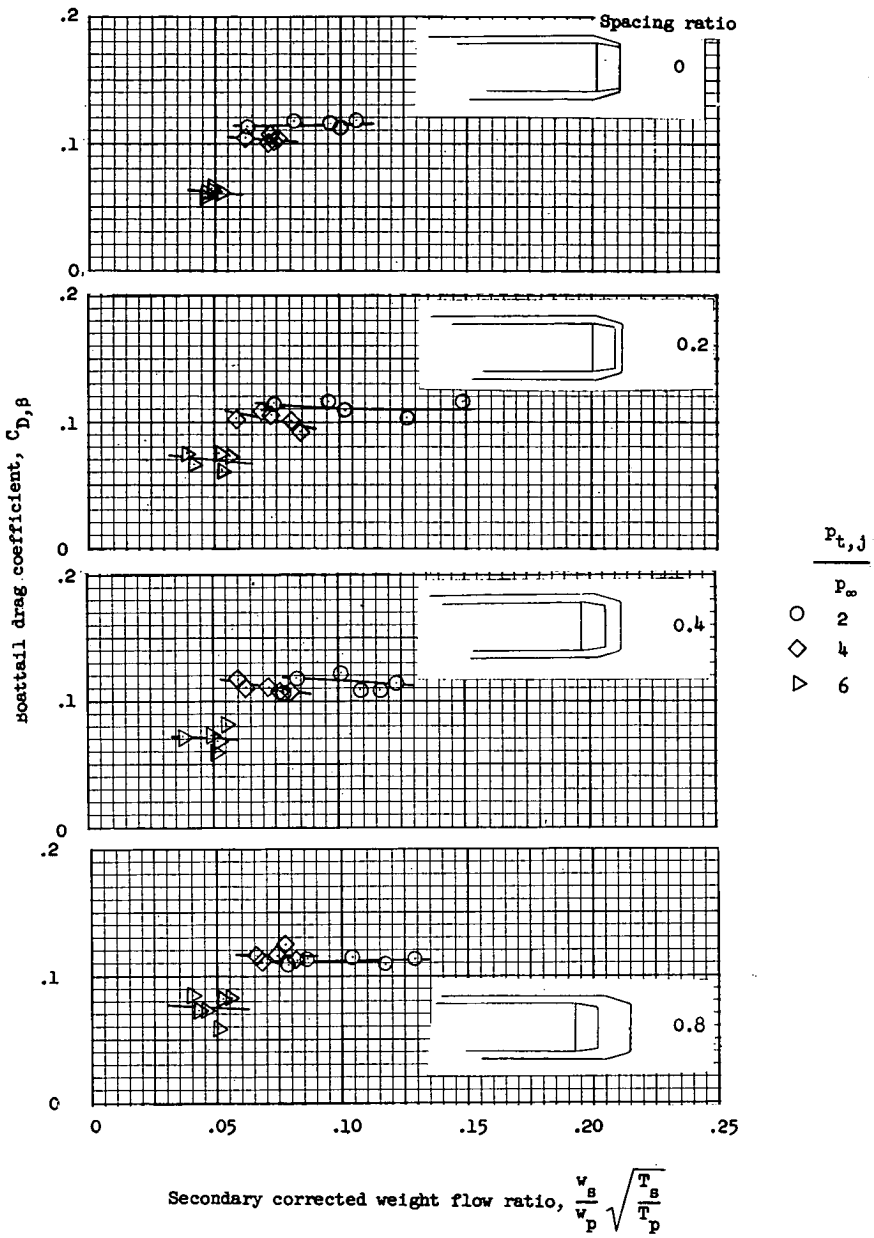

(a) $M_\infty = 0.9$.

Figure 7.- Variation of boattail drag coefficient with corrected weight flow ratio at constant values of primary jet total-pressure ratio and spacing ratio. $\frac{d_s}{d_p} = 1.10$.

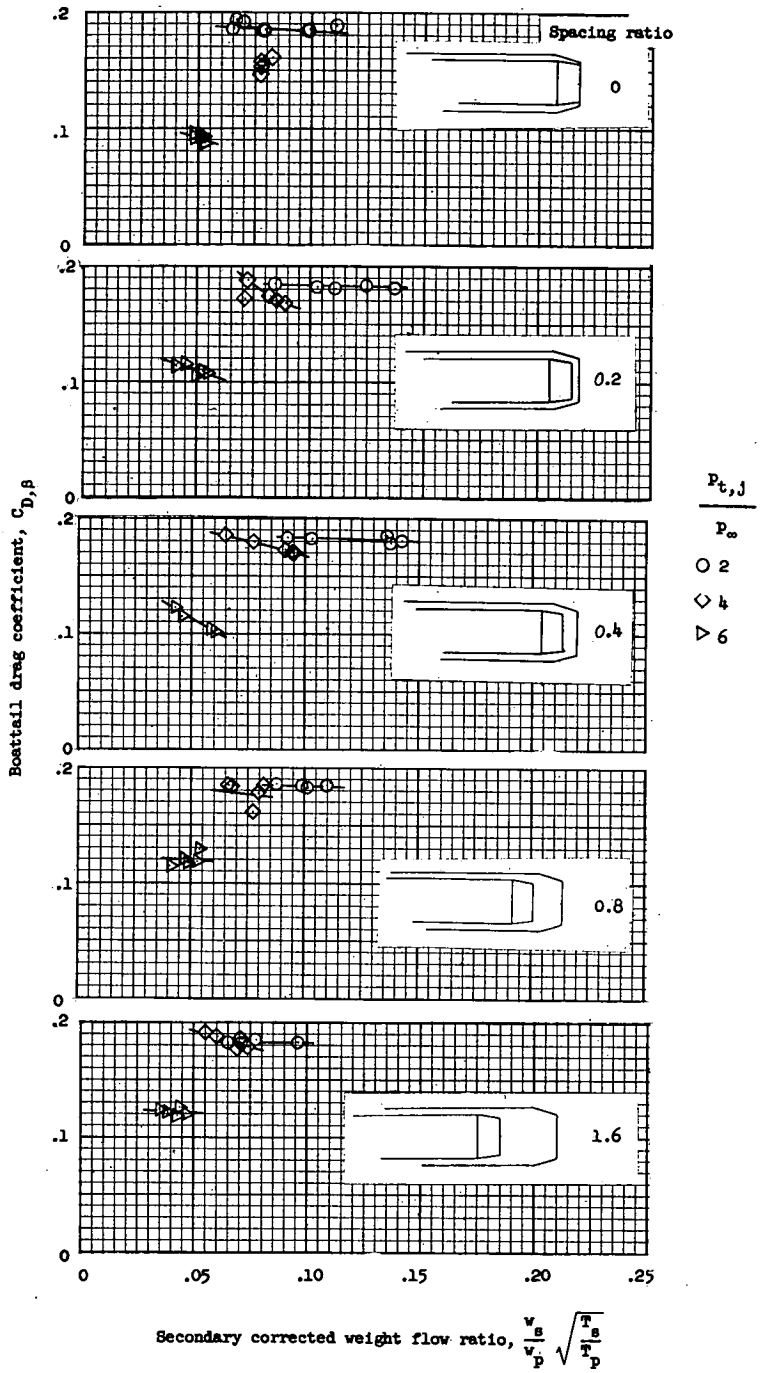

(b) $M_\infty = 1.10$.

Figure 7.- Continued.

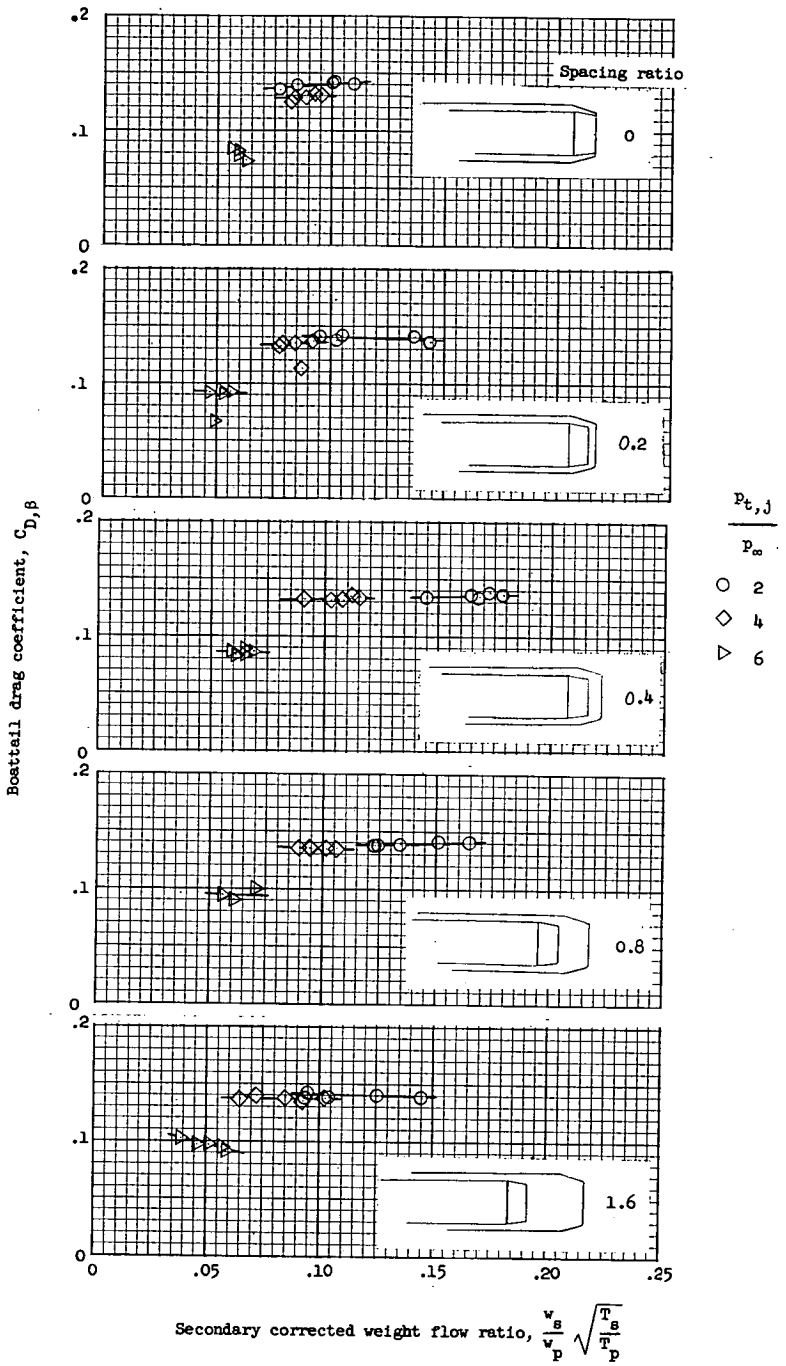

(c) $M_\infty = 1.26$.

Figure 7.- Concluded.

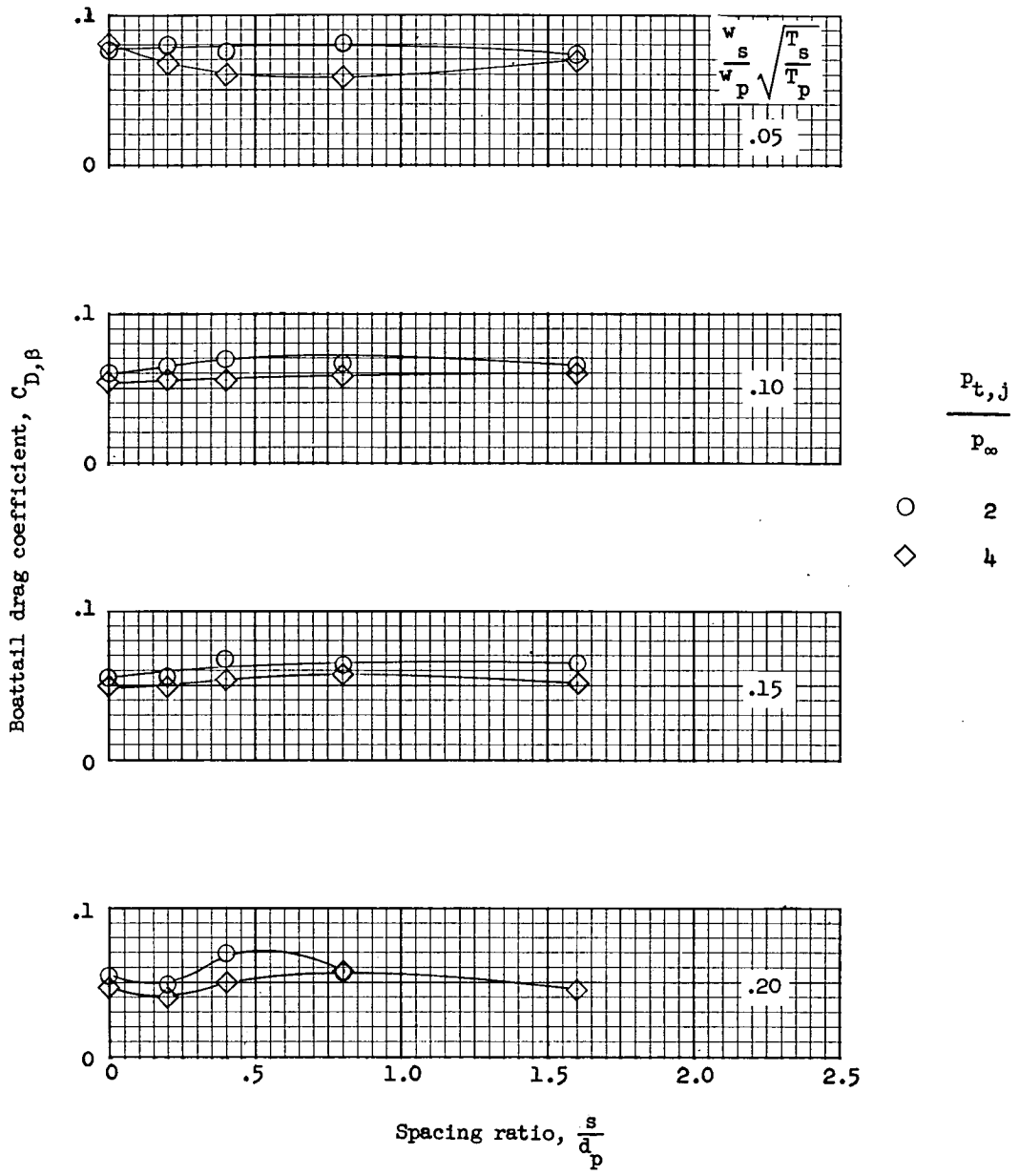

(a) $M_\infty = 0.6$.

Figure 8.- Variation of boattail drag coefficient with spacing ratio at constant values of primary jet total-pressure ratio and secondary mass flow. $\frac{d_s}{d_p} = 1.35$.

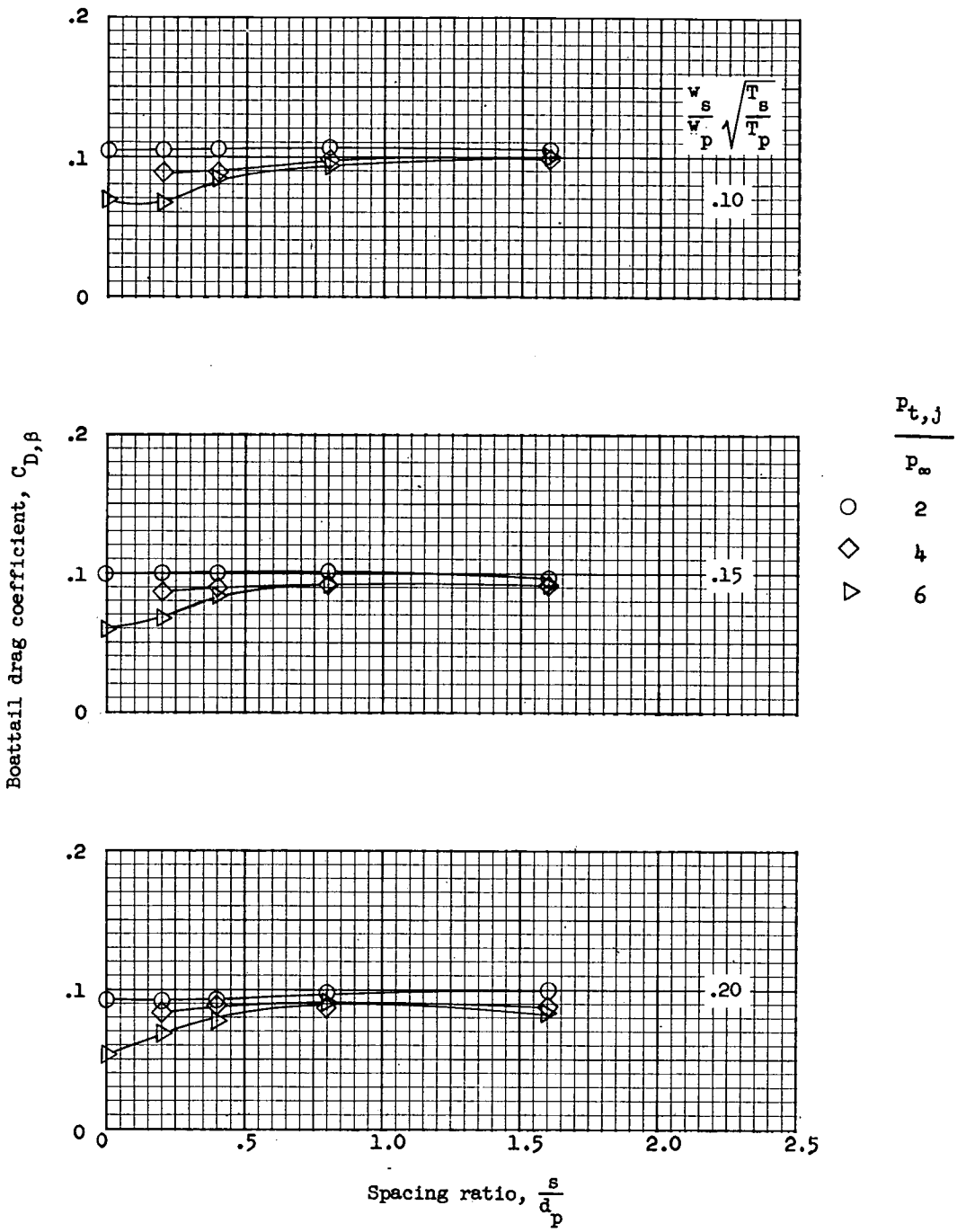

(b) $M_\infty = 0.9$.

Figure 8.- Continued.

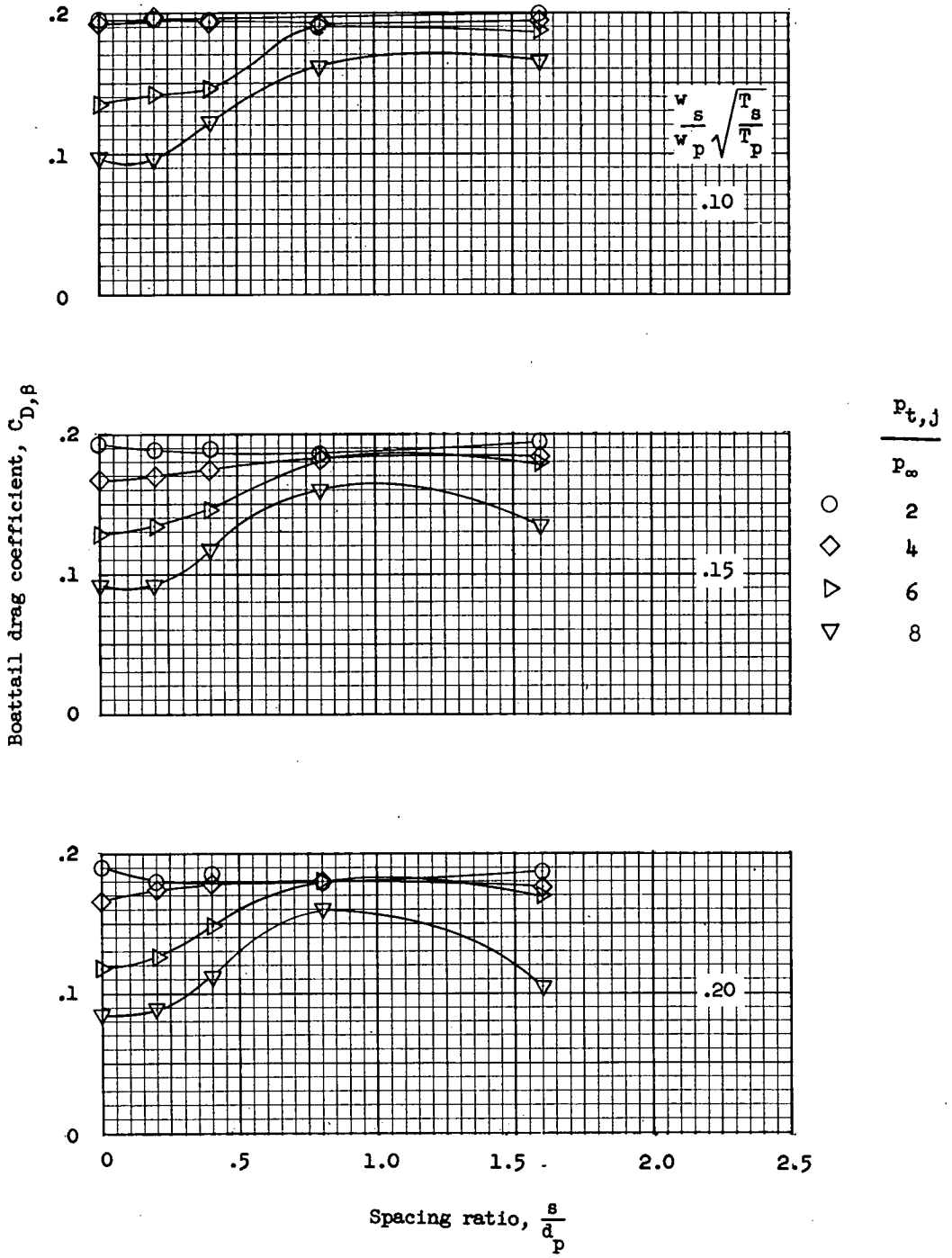

(c) $M_\infty = 1.10$.

Figure 8.- Continued.

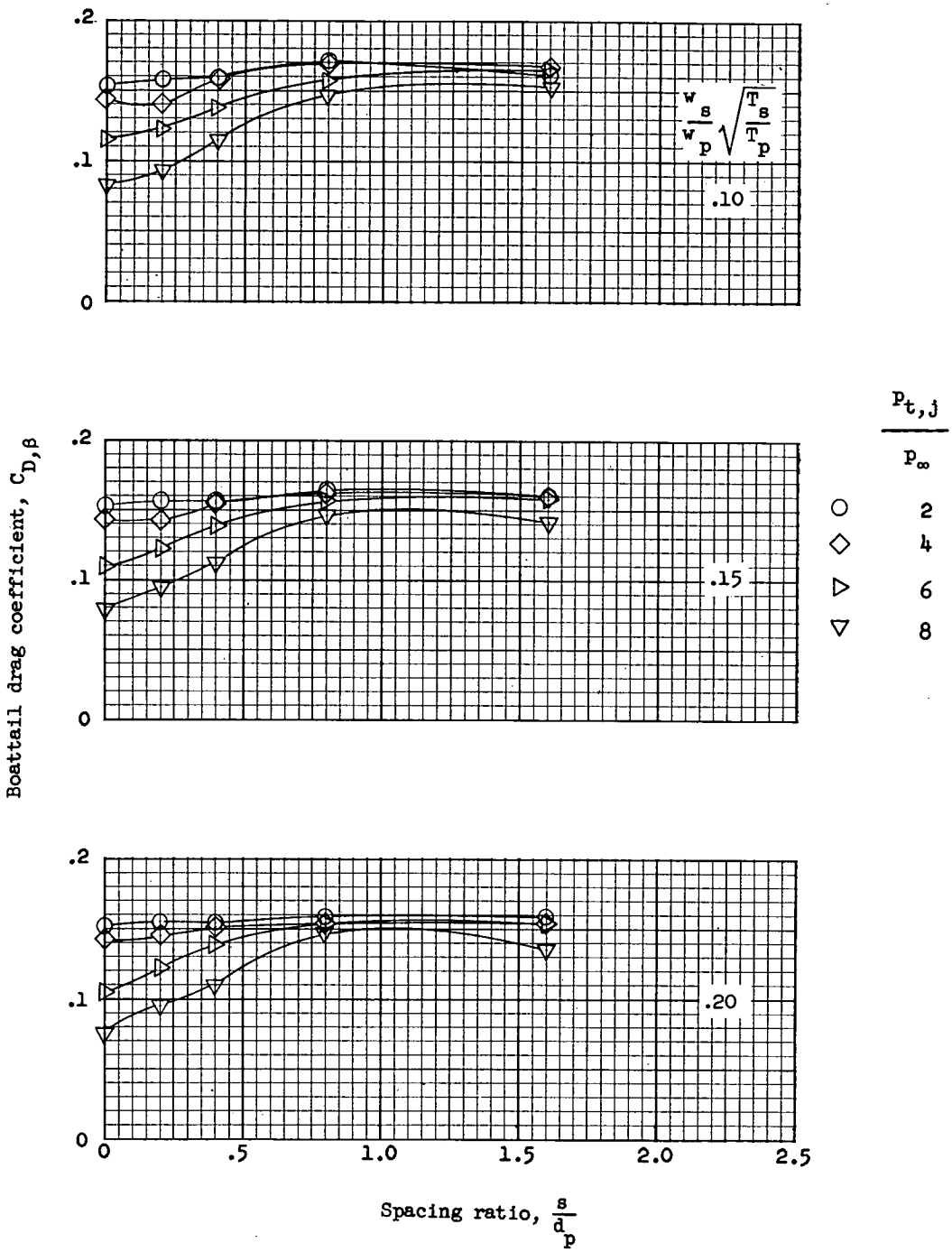

(d) $M_\infty = 1.26$.

Figure 8.- Concluded.

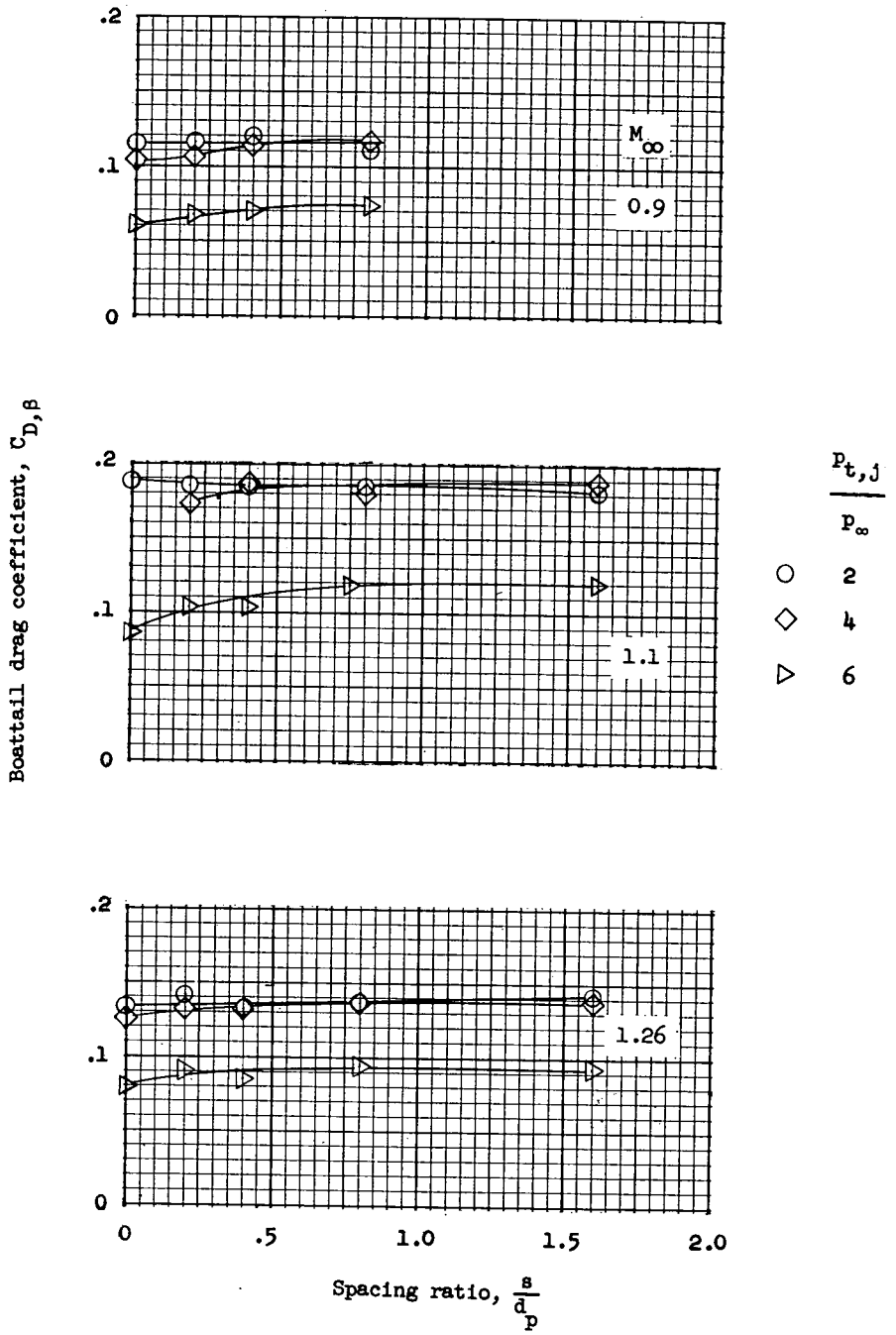

Figure 9.- Variation of boattail drag coefficient with spacing ratio at constant values of primary jet total-pressure ratio. $\frac{w_s}{w_p}\sqrt{\frac{T_s}{T_p}} = 0.06$; $\frac{d_s}{d_p} = 1.10$.

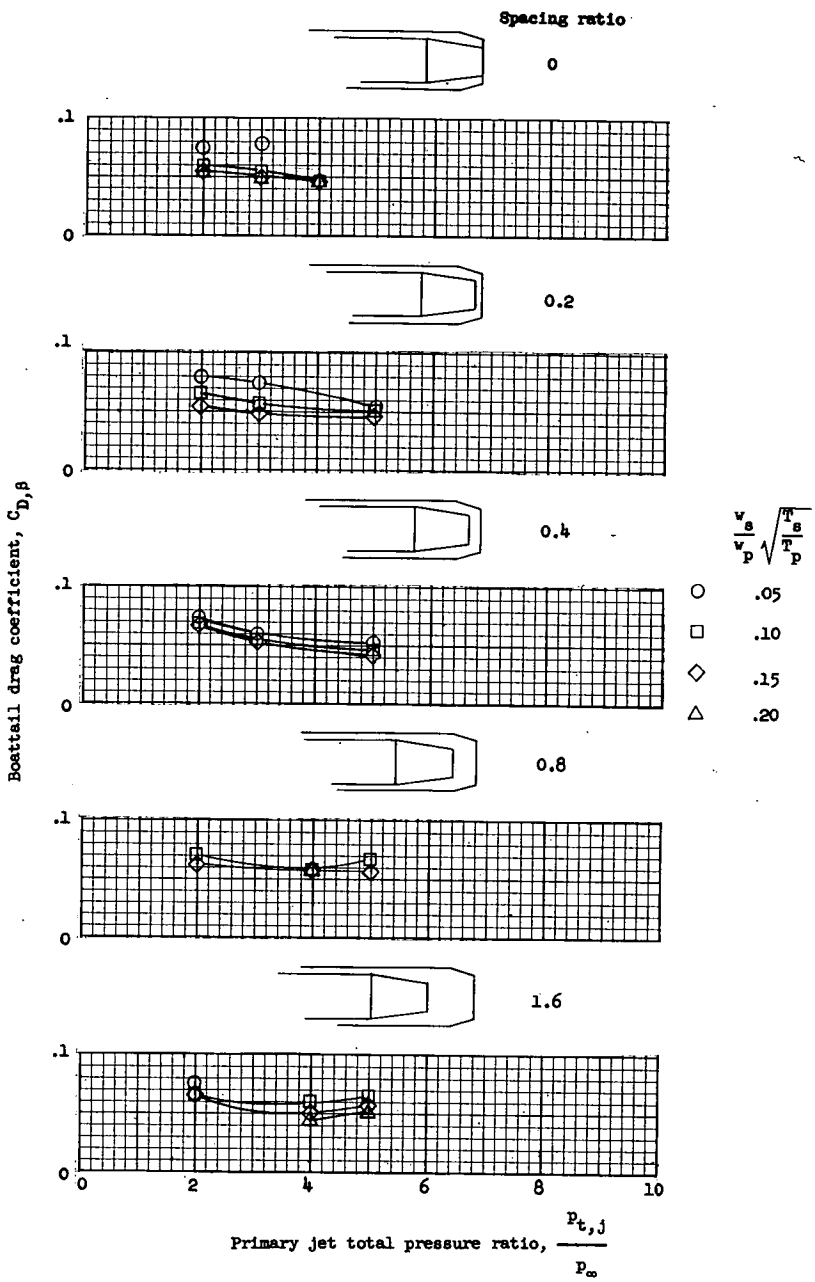

(a) $M_\infty = 0.6$.

Figure 10.- Variation of boattail drag coefficient with primary jet total-pressure ratio at constant values of corrected weight flow and spacing ratio. $\frac{d_s}{d_p} = 1.375$.

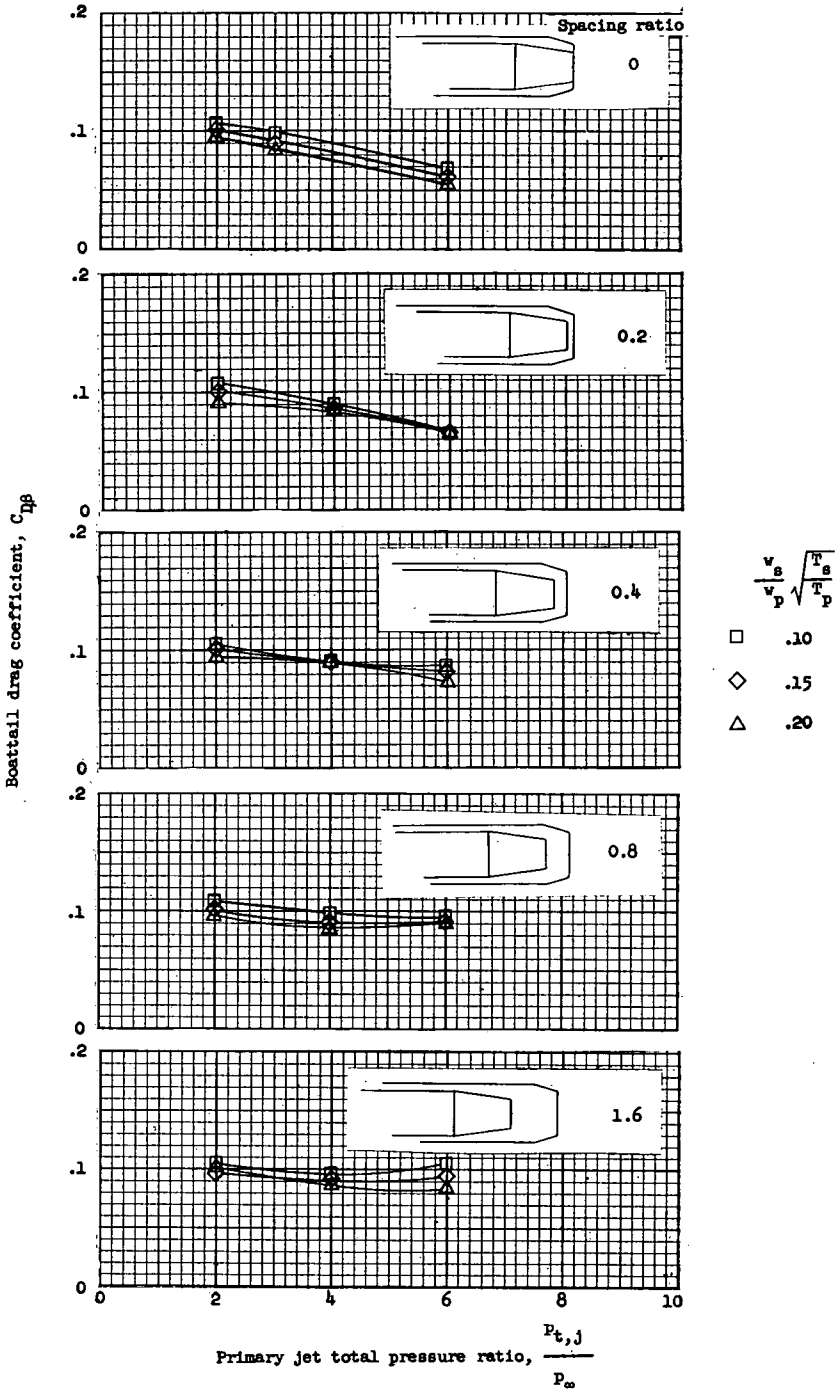

(b) $M_\infty = 0.9$.

Figure 10.- Continued.

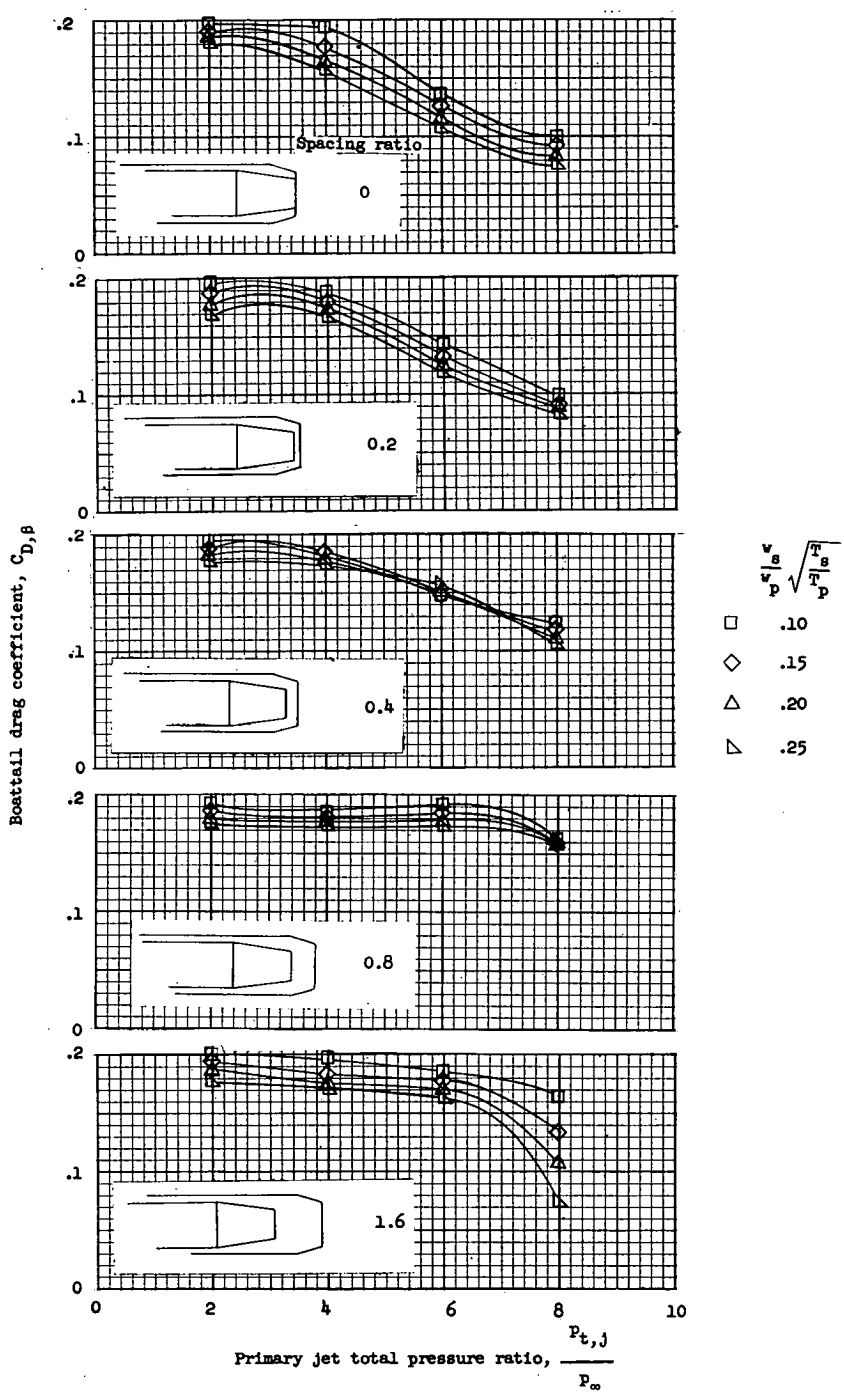

(c) $M_\infty = 1.10$.

Figure 10.- Continued.

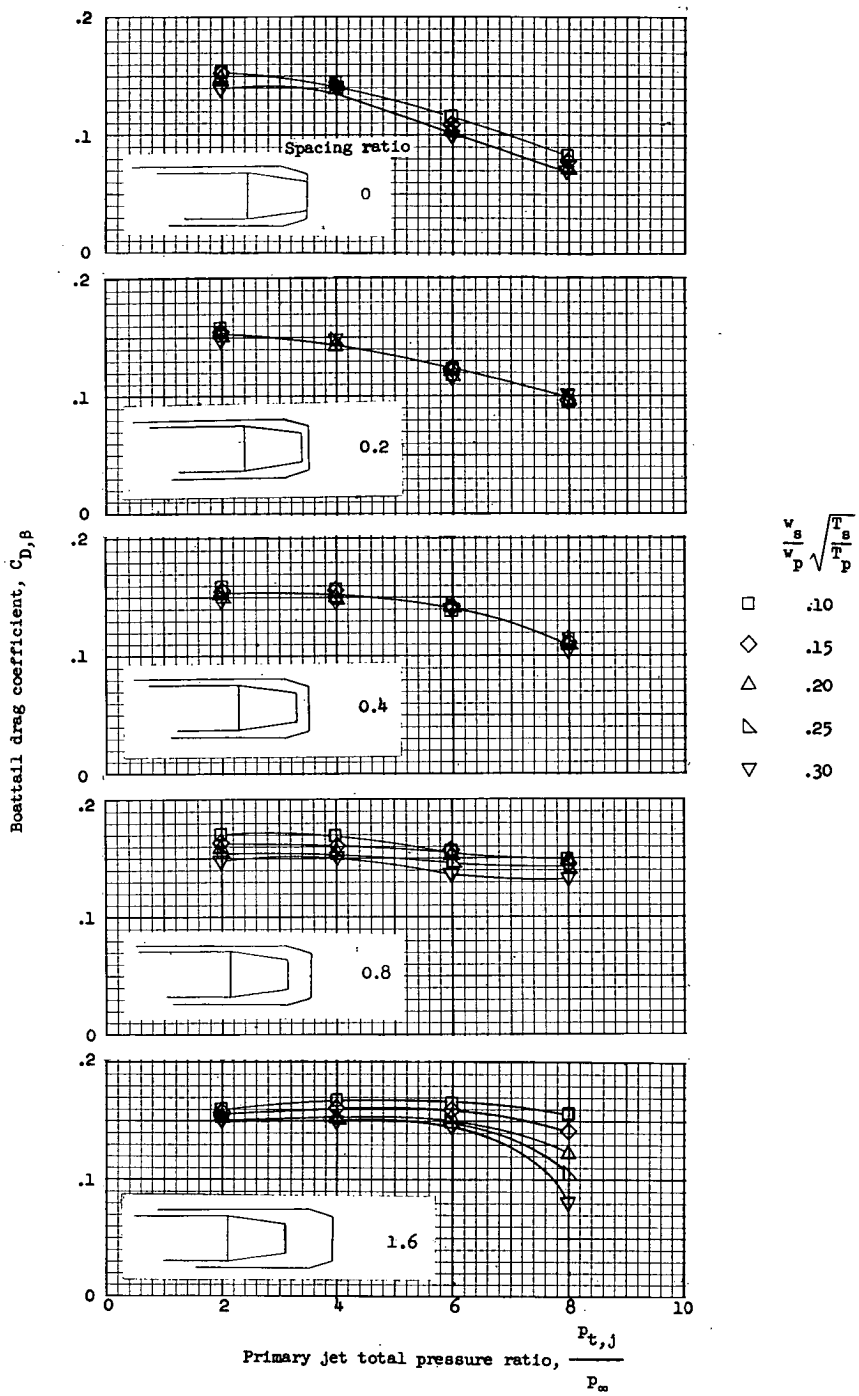

(d) $M_\infty = 1.26$.

Figure 10.- Concluded.

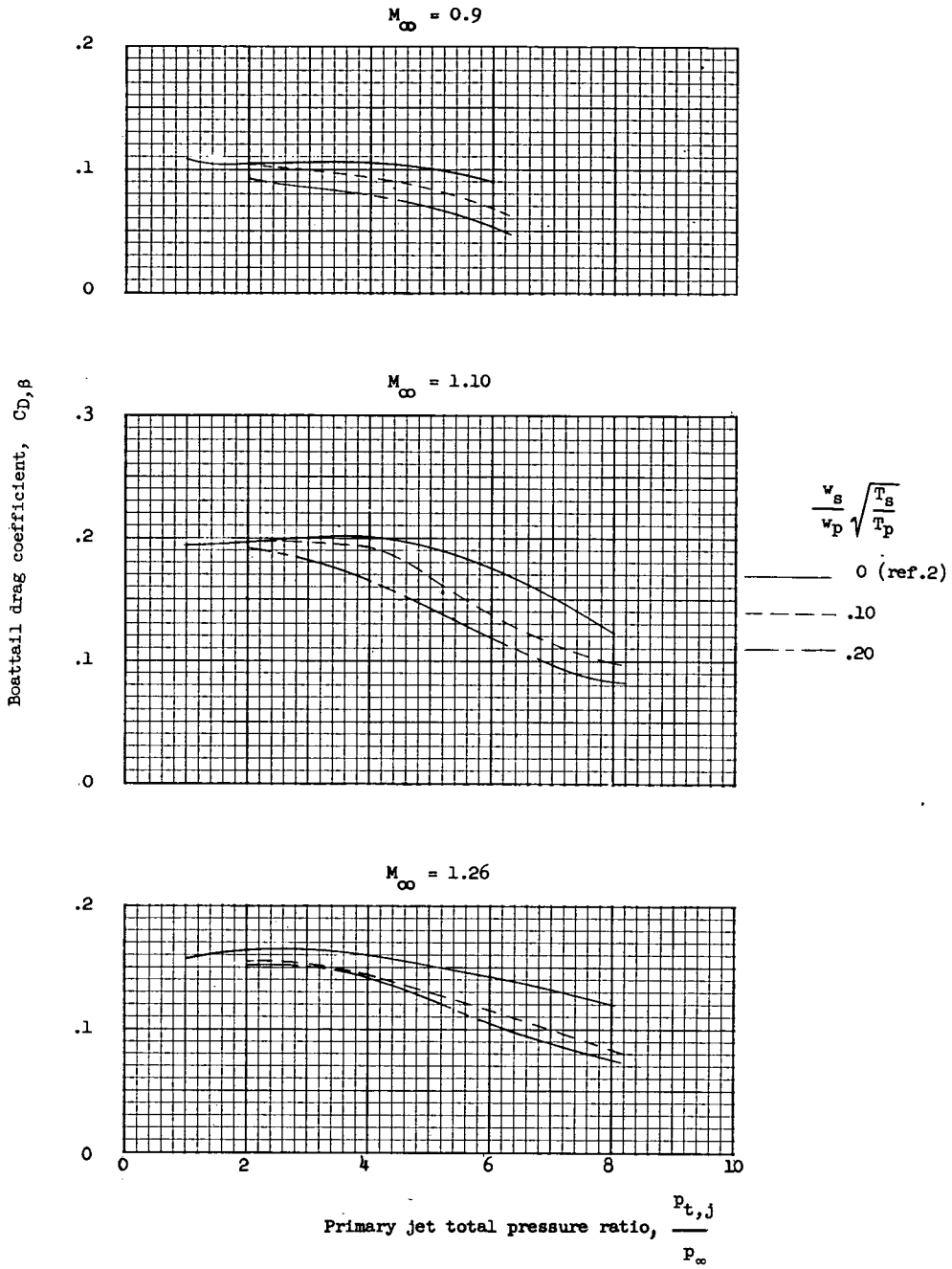

Figure 11.- Comparison with interpolated data from reference 2. $\frac{s}{d_p} = 0$; $\frac{d_b}{d_m} = 0.75$; $\frac{d_p}{d_b} = 0.67$; $\beta = 16^\circ$.